Construction of a superhydrophobic ZnO-rGO/CMF composite and its high-efficiency oil adsorption-separation performance

Yang Shifang, Yu Peng*

(*Key Laboratory for Photonic and Electronic Bandgap Materials*, *Ministry of Education*, *School of Physics and Electronic Engineering*, *Harbin Normal University Harbin* 150025, *China*)

Abstract: Oily wastewater discharge severely endangers the environment and hinders energy conservation efforts, necessitating the development of high-performance oil-water separation materials. We report the formation of a superhydrophobic and superoleophilic composite by integrating ZnO with reduced graphene oxide (rGO) on a carbonized melamine foam (CMF) using pristine melamine foam (MF) as the starting substrate. The fabrication involved two key steps: hydrothermal treatment and high-temperature pyrolysis. Characterization showed that the resultant ZnO-rGO/CMF composite had a water contact angle of 151.5°, indicating excellent superhydrophobicity. Both static adsorption and continuous dynamic separation tests verified the composite's superior oil-water separation performance. It had remarkable adsorption capacities for various oils and organic solvents, with a maximum adsorption capacity of 120.2 g/g for soybean oil, surpassing the values for most previously reported MF-derived carbon-based adsorbents. After 20 consecutive separation cycles, the composite maintained a stable adsorption performance, demonstrating good recyclability. It also had an excellent compression resistance and good flame retardancy. It retained 70% of its original adsorption capacity for gasoline after five combustion cycles, confirming its reusability under high-temperature conditions. Hydrophobic carbon-based porous sponges were developed, providing valuable insights for the design and development of advanced carbon-based superhydrophobic materials for environmental remediation, particularly in oily wastewater treatment.

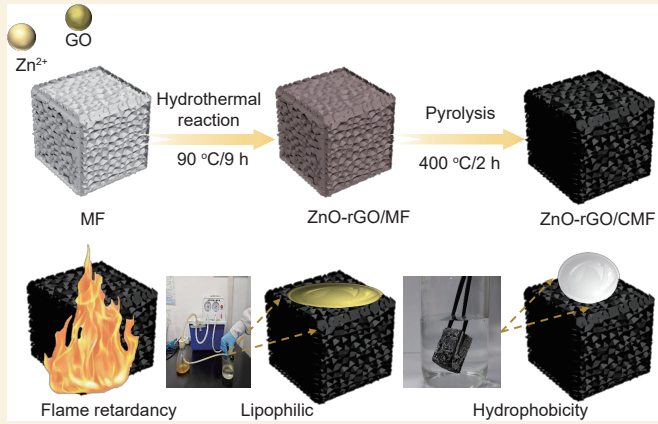

Key words: Melamine foam; Carbonization; Reduced graphene oxide; Oil-water separation; Superhydrophobic

1 Introduction

Frequent leakage accidents during petroleum extraction, transportation, and refining, along with the increasing discharge of industrial oily wastewater, have led to serious issues such as energy waste, environmental pollution, and ecological damage[1–2]. Meanwhile, oil pollutants in domestic sewage cause pipeline blockages by forming a floating oil layer on water surfaces, thereby hindering reoxygenation and disrupting ecological cycles[3]. Traditional oil-water separation methods, such as mechanical skimming, chemical dispersion, and biodegradation, generally suffer from drawbacks including low separation efficiency, potential secondary pollution, complicated operation, and high costs[4–8]. These limitations make it difficult to meet the practical demands of large-scale industrial oily wastewater treatment and domestic sewage purification in complex environments[9–12]. Therefore, there is an urgent need to develop novel materials capable of absorbing, removing, and transferring oil contaminants from water effectively.

Adsorption is an effective approach for oil-water separation. A material is considered suitable for oil-water separation if its surface exhibits opposite wettability toward oil and water[13]. Melamine foam (MF)

Received: December 16, 2025
Revised: March 01, 2026
Accepted: March 02, 2026

has emerged as a promising substrate for developing novel hydrophobic oil-absorbing materials due to its low cost, excellent elasticity, high thermal stability, outstanding flame retardancy and eco-friendliness[14–16]. However, pristine MF is amphiphilic. The lack of selective adsorption capacity for oil precludes meeting the requirements of oil-water separation. Thus, surface modification is essential to construct a superhydrophobic and superoleophilic interface[17]. Currently, carbonization under an inert gas atmosphere is used to remove hydrophilic groups (e.g., $-NH_2$, $-OH$) from the surface of MF, forming carbonized melamine foam (CMF) with significantly enhanced hydrophobicity and lipophilicity[18]. For instance, Niu et al. prepared superhydrophobic CMF by pyrolysis at 1000 °C, with an adsorption capacity of 60–150 g/g. However, the material exhibited poor adsorption performance for low-viscosity organic solvents at room temperature and required photothermal or Joule heating to achieve effective adsorption. Additionally, the impact of repeated heating-cooling cycles on its adsorption performance has not been evaluated[19]. Therefore, it is necessary to uniformly coat a well-designed carbon precursor on the skeleton of pristine MF to regulate the surface wettability and structural stability of the final material.

At present, two principal strategies are used to prepare superhydrophobic surfaces: (1) modifying rough surfaces with low surface energy substances and (2) constructing surface roughness on low surface energy materials[20]. Among these, reduced graphene oxide (rGO) has emerged as an ideal additive for fabricating hydrophobic composite oil-absorbing materials due to its inherently low surface energy[21]. For example, Duman et al. successfully fabricated a CMS/rGO/PFDT composite oil-absorbing material by modifying carbonized melamine sponge with rGO and 1H,1H,2H,2H-perfluorodecanol (PFDT), which exhibited excellent oil adsorption performance[22]. However, this approach has notable limitations. The process is complex and highly dependent on toxic chemicals and flammable reagents harmful to the environment, which pose environmental concerns and significantly restrict large-scale industrial applications. Zinc oxide (ZnO) offers notable advantages, including low preparation cost, high stability, environmental friendliness, and excellent flame retardancy, and is widely used as an auxiliary modification material. Previous studies have confirmed that adding nano-ZnO to GO films can increase the surface roughness, providing strong support for the construction of superhydrophobic structures[23].

Inspired by the superhydrophobic properties of the *Nelumbo nucifera* (lotus) leaf, commonly known as the Lotus Effect, this study combines the characteristics of low surface energy substances to realize the bionic replication of superhydrophobic surfaces of oil-absorbing materials by preparing micro-nano scale protrusions on the material surface. First, low surface energy rGO was uniformly coated on the melamine foam framework, and then ZnO was introduced to modify the composite material, successfully constructing a zinc oxide-reduced graphene oxide/carbonized melamine foam (ZnO-rGO/CMF) carbon-based composite sponge. To clarify the synergistic modification effects of rGO and ZnO, two control samples — rGO/carbonized melamine foam (rGO/CMF) and ZnO/carbonized melamine foam (ZnO/CMF) —were prepared. The effects of composite modification on microstructure, wettability, oil adsorption capacity, and cyclic stability were systematically investigated. Ultimately, a composite oil-absorbing material with excellent hydrophobicity, lipophilicity, and structural stability was developed, providing a promising strategy for oil-water separation.

2 Materials and method

2.1 Materials and reagents

Melamine foam (MF) was used as the substrate. Expanded graphite, sodium nitrate, concentrated sulfuric acid, potassium permanganate, 30% hydrogen peroxide solution, hydrochloric acid, and ethanol were used to prepare graphite oxide (GO). Zinc nitrate, hexamethylenetetramine (HMT), ammonia solution (5%, *v*/*v*), polyvinylpyrrolidone, anhydrous ethanol, and deionized water were used for composite modific-

ation. All chemicals were of analytical grade and used without further purification. Soybean oil, n-hexane, gasoline, acetone, dimethylformamide (DMF), and petroleum were used as test liquids in adsorption experiments.

2.2 Material preparation

2.2.1 Preparation of GO

1.0 g of sodium nitrate and 0.5 g of expanded graphite were added to a beaker, followed by the slow addition of 25 mL of concentrated sulfuric acid. The mixture was stirred vigorously for 30 min to ensure thorough mixing. The beaker was then placed in a water bath for heating. During heating, 3.0 g of potassium permanganate was added in batches under continuous stirring, and the reaction was maintained for 24 h. After completion of the reaction, 40 mL of distilled water was added in portions under stirring to avoid local overheating. After the solution cooled naturally, 30% (*v*/*v*) hydrogen peroxide was added dropwise until the solution turned golden yellow and no further bubbles were observed, indicating the completion of the reaction. Finally, the resulting product was washed alternately with hydrochloric acid and ethanol three times and then dried at room temperature to obtain GO.

2.2.2 Preparation of rGO/CMF

MF was repeatedly washed with deionized water to remove impurities from its surface and pores, and then dried in an oven at 80 °C for 12 h. The prepared GO was dispersed in anhydrous ethanol and ultrasonicated to obtain homogeneous GO ethanol solutions of different concentrations. The dried MF was immersed in the GO ethanol solution for 1 h, then removed and dried in an oven for 12 h, resulting in uniform loading of GO onto the foam skeleton. Finally, the dried foam was placed in a tube furnace, heated to 400 °C at a rate of 2 °C/min under a nitrogen atmosphere, and pyrolyzed for 2 h to obtain rGO/CMF.

2.2.3 Preparation of ZnO-rGO/CMF

GO exhibits amphiphilic characteristics, with a gradient distribution from hydrophilic edges to a relatively hydrophobic basal plane, which reduces interfacial energy and enhances the compatibility of composite systems effectively[24−25]. The introduction of ZnO further improves the structural stability of the material. 0.2975 g of $Zn(NO_3)_2$ and 0.1402 g of HMT were dissolved in 40 mL of deionized water and stirred for 30 min to obtain a clear solution. Subsequently, 5% ammonia solution was added dropwise to adjust the pH to 10, yielding Solution A. Meanwhile, 40 mg of GO was dispersed in 40 mL of anhydrous ethanol and ultrasonicated for 30 min to obtain a homogeneous Solution B. Solution B was slowly added to Solution A, followed by the addition of 1 g of PVP as a dispersant and binder. Subsequently, MF was introduced, and the mixture was stirred for 30 min to ensure thorough impregnation of the foam. The resulting mixture was transferred into a reaction vessel and subjected to hydrothermal treatment at 90 °C for 9 h. After the hydrothermal reaction, the sponge was removed and dried in an oven. Finally, the dried material was placed in a tube furnace and pyrolyzed at 400 °C for 2 h under a nitrogen atmosphere to obtain superhydrophobic and superoleophilic ZnO-rGO/CMF (Fig. 1a).

2.3 Characterization and performance testing

2.3.1 Characterization

The surface and internal morphologies of pristine MF, CMF, rGO/CMF, ZnO/CMF, and ZnO-rGO/CMF were observed using a scanning electron microscope (SEM, SU-70). The microstructure of ZnO-rGO/CMF was further analyzed by transmission electron microscopy (TEM) and high-resolution transmission electron microscopy (HRTEM, TF-20). The elemental distribution on the sponge surface was characterized by energy-dispersive spectroscopy (EDS, TF-20). X-ray diffraction (XRD, D/max-2600/pc) was employed to analyze the crystal structure of ZnO-rGO/CMF and to confirm the presence of ZnO and carbon components. Raman spectroscopy (HR-800) was used to evaluate the structural order of the materials by analyzing the intensity ratio of the *D* band to the *G* band. The specific surface area was measured using an automatic surface area (ASAP 2460).

2.3.2 Performance testing

The water contact angles (WCA, OCA-20) of pristine MF, CMF, rGO/CMF, ZnO/CMF, and ZnO-

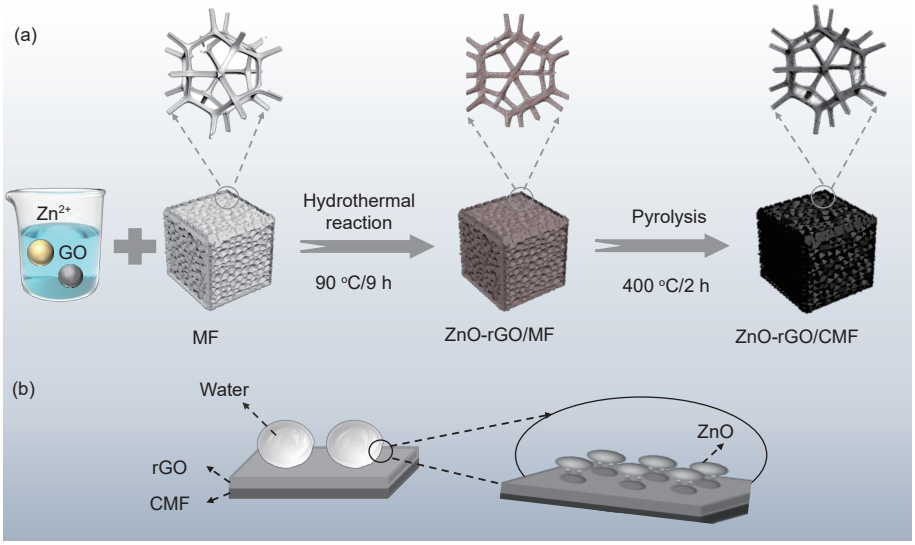

Fig. 1 (a) Schematic diagram of ZnO-rGO/CMF sponge material synthesis. (b) Synergetic wetting mechanism diagram

rGO/CMF were measured using a contact angle goniometer. Hydrophobicity was further evaluated by observing the morphology of water droplets and by performing an underwater silver mirror effect test.

A 200 g weight was applied to each sponge sample and maintained for 20 s to ensure continuous compression. After removal of the weight, the heights of the sponge before and after compression were measured using a steel ruler to evaluate compression resistance and recovery performance.

Oil-water separation tests were conducted to evaluate the performance of MF and ZnO-rGO/CMF. An oil-water mixture was prepared in a beaker, and the materials were immersed to observe their adsorption behavior. After separation, the aqueous phase was examined using an optical microscope to detect residual oil droplets. To further assess the continuous separation performance, a vacuum-assisted filtration system was constructed. ZnO-rGO/CMF was fixed at one end of a hose immersed in the oil-water mixture, while the other end was connected to a collection vessel via a vacuum pump.

The adsorption capacity of ZnO-rGO/CMF for soybean oil, n-hexane, gasoline, acetone, dimethylformamide (DMF), and petroleum were evaluated using the gravimetric method. The sponge sample (1.5 cm × 1.5 cm × 4 cm) was immersed in 30 mL of the target oil or organic solvent until saturation. To minimize evaporation, the saturated sponge was immediately removed, and excess liquid on the surface was allowed to drain before weighing. The adsorption capacity (Q) was calculated using the following equation:

$$Q = \frac{M_1 - M_0}{M_0}$$

where Q: adsorption capacity (g/g), representing the mass of oil/organic solvent adsorbed per unit mass of dry sponge material. M_0: dry mass of the sponge material before adsorption (g). M_1: total mass of the sponge material after saturation with oil/organic solvent and surface draining of excess liquid (g).

After squeezing the oil- and organic solvent-saturated ZnO-rGO/CMF, the samples were thoroughly washed with anhydrous ethanol. The samples were then dried at 60 °C for 2 h prior to cyclic adsorption tests to evaluate their reusability. The adsorption-squeezing-drying cycle was repeated 20 times, and the adsorption capacity for each cycle was calculated using the aforementioned equation.

Thermogravimetric analysis (TGA) was conducted using a Discovery TGA55 analyzer under a nitrogen atmosphere at a heating rate of 10 °C/min over a temperature range of 30–900 °C. Combustion experiments were conducted to evaluate the structural stability and reusability of ZnO-rGO/CMF after gasoline adsorption. Specifically, ZnO-rGO/CMF was subjected to 5 combustion cycles. Each cycle consisted of exposure to a flame for 60 s, followed by self-extin-

guishing and cooling to room temperature. After each cycle, the adsorption capacity for gasoline was measured to evaluate the retention of adsorption performance. To evaluate flame retardancy, the sample was subjected to five consecutive combustion tests, each lasting 10 s. The surface condition after combustion was observed and recorded. The flammability rating was determined according to the UL-94 standard.

3 Results and discussion

3.1 Surface morphology and chemical composition

In this work, rGO was coated onto the CMF framework to construct a microscale rough surface, while nanoscale ZnO was further introduced to enhance surface roughness. This hierarchical structure enables air trapping when water droplets contact the surface, forming a thin air layer between the droplets and the material. As a result, water droplets contact only the surface protrusions, and the surface tension of water exceeds the adhesive force between water and the material surface (Fig. 1b). Consequently, water droplets adopt a nearly spherical shape, resulting in superhydrophobic behavior. The surface microstructure plays a crucial role in determining material performance. SEM was employed to characterize the morphologies of pristine MF, CMF, rGO/CMF, ZnO/CMF, ZnO-rGO/MF, and ZnO-rGO/CMF (Fig. 2). As shown in Fig. 2a, pristine MF exhibited a typical three-dimensional interconnected porous structure with a smooth skeleton surface and uniform pore distribution. After carbonization, CMF displayed a slightly roughened skeleton surface while maintaining its porous structure (Fig. 2b). For rGO/CMF (Fig. 2c), the skeleton surface was covered with wrinkled and layered rGO sheets, significantly increasing surface roughness. Fig. 2d exhibites granular protrusions on the skeleton surface, corresponding to ZnO nanoparticles. ZnO-rGO/MF (Fig. 2e) and ZnO-rGO/CMF (Fig. 2f) exhibited both layered rGO structures and ZnO nanoparticle protrusions. Notably, ZnO-rGO/CMF showed a more compact skeleton and a more uniform distribution of the composite components. The combination of micro/nano-scale roughness and a porous structure not only preserves the oil storage capacity of the material but also enhances its hydrophobicity[26]. TEM and HRTEM analyses (Fig. 2g-h) revealed that ZnO nanoparticles were tightly anchored onto the rGO sheets within ZnO-rGO/CMF. The chemical composition of ZnO-rGO/CMF was further analyzed by EDS mapping (Fig. 2i-l). The elemental mapping images show a uniform distribution of C, N, O, and Zn elements throughout the material, confirming the successful formation of the composite.

The crystalline structures of ZnO, rGO/CMF, and ZnO-rGO/CMF were analyzed by XRD (Fig. 3). The XRD pattern of ZnO-rGO/CMF exhibited a series of diffraction peaks at 2θ values of 31.79°, 34.4°, 36.2°, 47.5°, 56.5°, 62.8°, 66.3°, 67.9°, 69°, 72.5°, and 76.9°, corresponding to the (100), (002), (101), (102), (110), (103), (200), (112), (201), (004), and (202) crystal planes of ZnO, respectively. These peaks confirm the formation of hexagonal wurtzite ZnO in the composite. A broad diffraction peak around 26° corresponds to the (002) plane of graphitic carbon, confirming the presence of rGO in the composite (Fig. 3a). The relatively low intensity of ZnO peaks compared to the carbon peak may be attributed to the dominant carbon matrix derived from MF. Further verification of the structural order of ZnO-rGO/CMF was conducted by Raman spectroscopy. The Raman spectra showed a characteristic ZnO peak at 434.2 cm^{-1}, along with the carbon material's *D* peak at 1350 cm^{-1} and *G* peak at 1596.4 cm^{-1}. The I_D/I_G ratio of ZnO was 0.82, lower than that of rGO/CMF (0.9), indicating that the introduction of ZnO enhanced the structural order of the material. The *G*-band in the Raman spectrum of ZnO-rGO/CMF exhibited a slight shift compared with rGO/CMF. This was caused by local lattice distortion induced by ZnO doping, which further confirmed the successful incorporation of ZnO (Fig. 3b). XRD and Raman spectra showed that ZnO was successfully composited on the rGO/CMF substrate, and the crystal structure of ZnO and the carbon structure of rGO were retained after compositing.

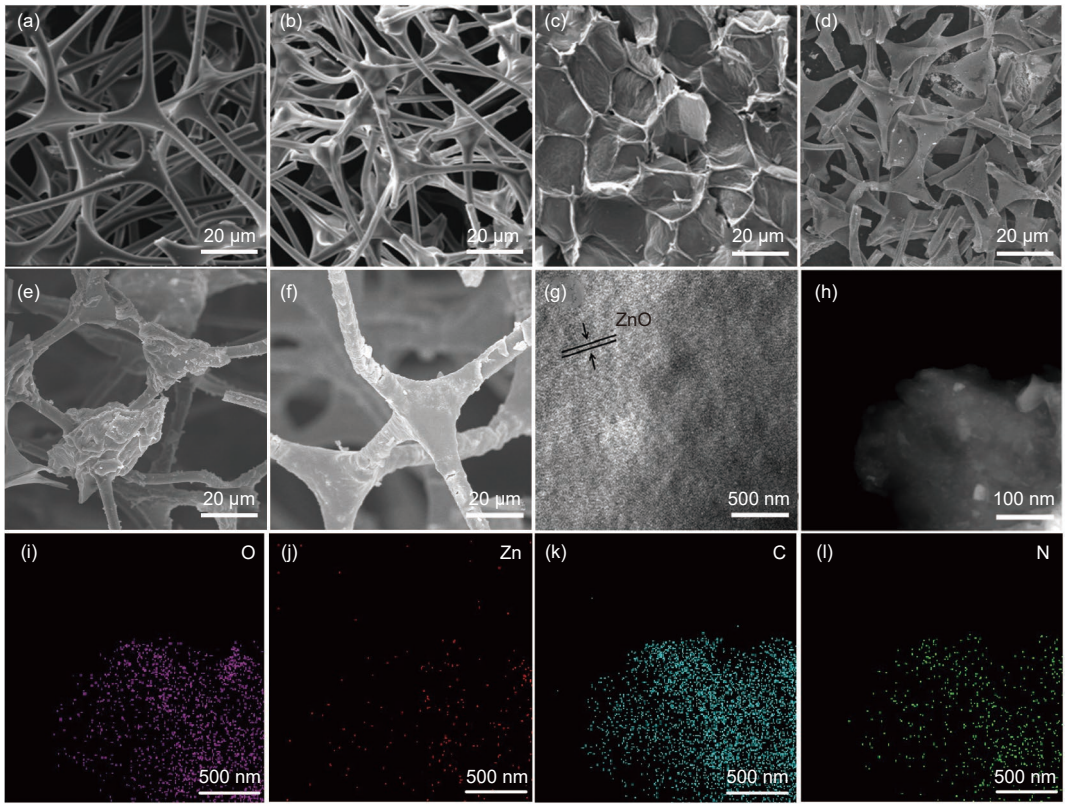

Fig. 2 SEM images of (a) pristine MF, (b) CMF, (c) rGO/CMF, (d) ZnO/CMF, (e) ZnO-rGO/MF and (f) ZnO-rGO/CMF. TEM images of (g) ZnO-rGO/CMF and (h) ZnO-rGO/CMF. (i-l) EDS mapping images of O, Zn, C and N elements corresponding to ZnO-rGO/CMF

3.2 Material properties

3.2.1 Hydrophobicity

WCA is a key parameter for evaluating the wettability of functional materials and their oil-water separation performance. Water and oil droplets readily spread on the surface of pristine MF, indicating its amphiphilic nature. In contrast, water droplets on ZnO-rGO/CMF exhibited a nearly spherical shape, while oils and organic solvents were rapidly absorbed (Fig. 4a). When immersed in water, ZnO-rGO/CMF exhibited a distinct underwater silver mirror effect, further confirming its superhydrophobicity and superoleophilicity[27] (Fig. 4b). When placed on the surface of plant leaves, no visible damage was observed after removal, indicating its non-corrosive and environmentally benign nature (Fig. 4c). As shown in Fig. 4d, the WCA of pristine MF and CMF was 0°, indicating superhydrophilicity. After the introduction of rGO, the WCA of rGO/CMF increased significantly to 126°. In contrast, ZnO/CMF exhibited a WCA of 49°. The

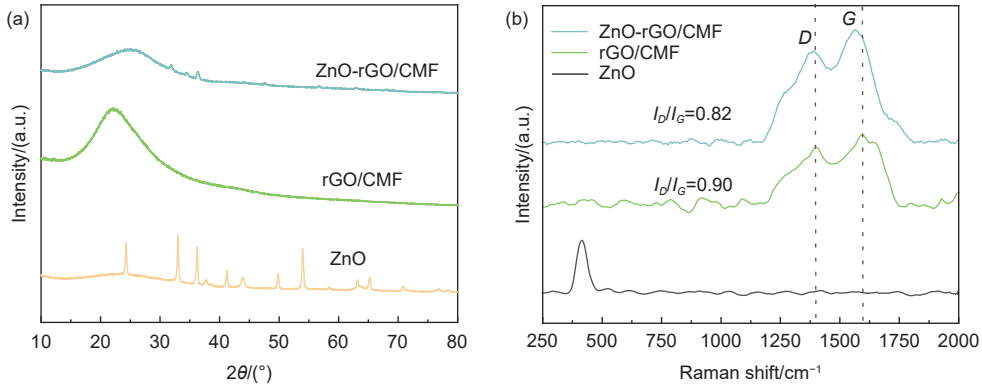

Fig. 3 (a) XRD patterns and (b) Raman spectra of ZnO, rGO/CMF and ZnO-rGO/CMF

WCA of ZnO-rGO/CMF further increased to 152°, demonstrating that the synergistic effect of rGO and ZnO significantly enhanced surface hydrophobicity. Water droplets were observed to roll off rapidly from the inclined surface of ZnO-rGO/CMF (Fig. 4e), indicating a low sliding angle. Therefore, ZnO-rGO/CMF exhibits both superhydrophobicity and superoleophilicity, providing a solid foundation for its application in oil-water separation.

3.2.2 Resistance to mechanical compression and recovery performance

In practical applications, ZnO-rGO/CMF is subjected to repeated compression and deformation. To evaluate its elasticity and structural stability, compression-recovery tests were performed. The initial height of rGO/CMF was 1.50 cm, which decreased to 0.60 cm under compression (Fig. S1) and recovered to 1.29 cm after unloading, corresponding to a recovery ratio of approximately 86% (Fig. 4f). In contrast, ZnO-rGO/CMF was compressed to 0.86 cm under the same load and recovered to 1.40 cm after unloading, which is closer to its original height (Fig. 4g). The stress-strain curve of ZnO-rGO/CMF is shown in Fig. S2. ZnO-rGO/CMF exhibited a compressive strain of 48% under a stress of 10 kPa, with a residual deformation of less than 2% after unloading. These results demonstrate that ZnO-rGO/CMF exhibits superior mechanical performance in terms of structural stability, recovery ability, and compression resistance compared to its counterparts. Photographs of the compression and recovery processes are provided in the supplementary materials.

3.2.3 Oleophilicity and adsorption performance

Static adsorption experiments were conducted to evaluate the oil adsorption capacity of ZnO-rGO/CMF (Fig. 5a, 5b). As shown in Fig. 5a, pristine MF absorbed both water and soybean oil simultaneously, thus failing to achieve selective oil-water separation. In contrast, ZnO-rGO/CMF selectively adsorbed soybean oil from the water surface without absorbing water, demonstrating excellent oil-water selectivity. The appearance of the aqueous phase after adsorption by pristine MF and ZnO-rGO/CMF was visually examined (Fig. 5c, 5d). Residual oil droplets were observed in

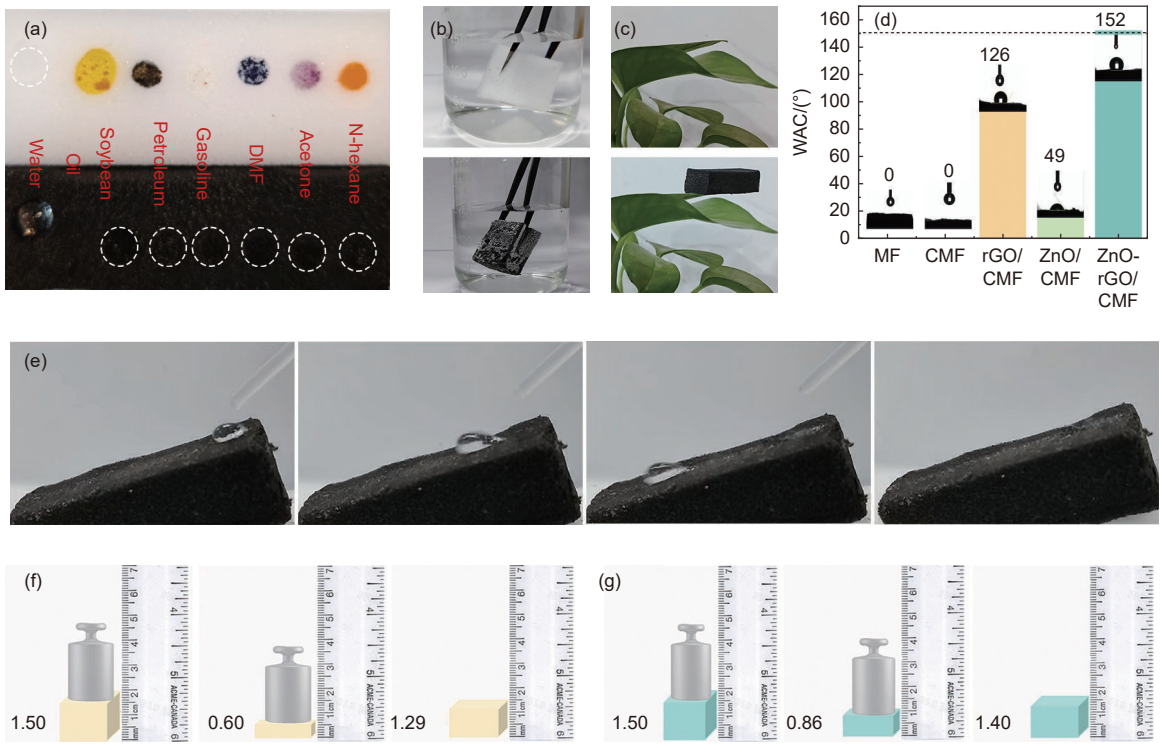

Fig. 4 (a) Images of water droplets and target substances on MF and ZnO-rGO/CMF. (b) Images of MF and ZnO-rGO/CMF placed in a beaker. (c) Image of ZnO-rGO/CMF placed on a green plant. (d) Water contact angles (WCAs) of MF, CMF, rGO/CMF, ZnO/CMF and ZnO-rGO/CMF. (e) Process of water droplets rolling off the inclined surface of ZnO-rGO/CMF. Pressure recovery test of (f) rGO/CMF and (g) ZnO-rGO/CMF sponge materials

the aqueous phase after treatment with pristine MF, whereas the solution became clear after treatment with ZnO-rGO/CMF. These results indicate that ZnO-rGO/CMF exhibits superior adsorption performance and selectivity toward soybean oil. Additionally, a continuous oil-water separation experiment was conducted (Fig. 5e). A hose with ZnO-rGO/CMF fixed at one end was immersed in the oil-water mixture, while the other end was connected to a vacuum pump. Soybean oil was rapidly absorbed by ZnO-rGO/CMF and efficiently transported to a collection container via vacuum suction within 20 s.

rGO with low surface energy was uniformly coated onto the MF framework to construct a hydrophobic surface. ZnO was subsequently introduced to increase surface roughness and construct a micro/nano hierarchical structure, thereby imparting excellent water repellency. In addition, the intrinsic lipophilicity of ZnO endows the ZnO-rGO/CMF composite with rapid oil-water separation capability. The incorporation

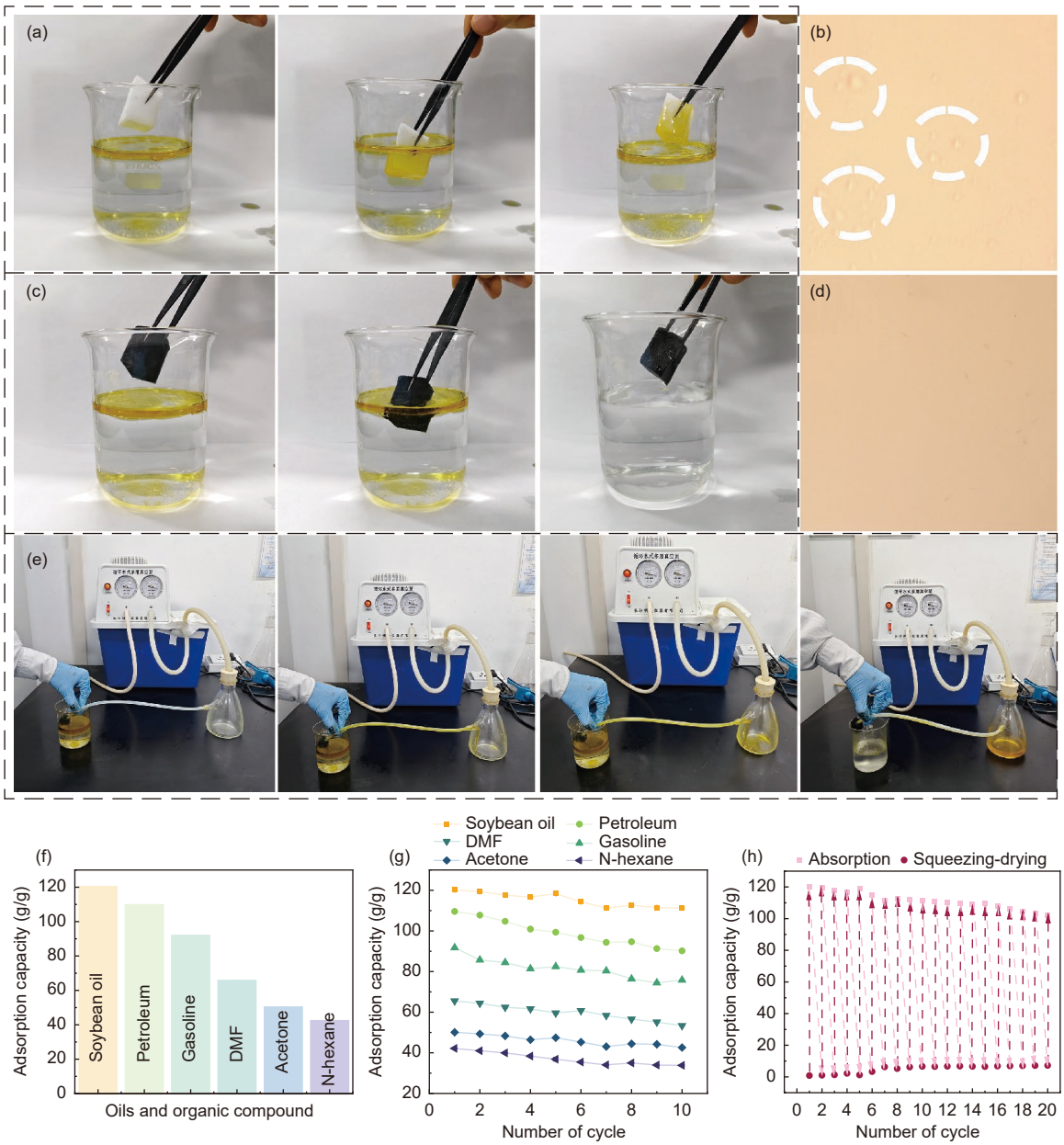

Fig. 5 (a, c) Static adsorption processes of soybean oil by pristine MF and ZnO-rGO/CMF. (b, d) Optical microscopic images of aqueous solutions after soybean oil adsorption by MF and ZnO-rGO/CMF. (e) Demonstration of continuous oil water separation process of ZnO-rGO/CMF. (f) Adsorption capacities of ZnO-rGO/CMF for various target substances. (g) Changes in adsorption capacities of ZnO-rGO/CMF for target substances after 10 adsorption-desorption cycles. (h) 20 adsorption-desorption cycle processes of ZnO-rGO/CMF for soybean oil

of rGO and ZnO significantly increases the specific surface area, providing more active sites for oil adsorption. As shown in Fig. S3, the specific surface area of ZnO-rGO/CMF is 19.8 m^2 g^{-1}, which is markedly higher than that of MF (18.1 m^2 g^{-1}). Soybean oil, n-hexane, gasoline, acetone, DMF, and petroleum were selected as model adsorbates to evaluate the adsorption performance of ZnO-rGO/CMF (Fig. 5f). The results demonstrate that ZnO-rGO/CMF exhibits excellent adsorption capacity toward a wide range of oils and organic solvents. The adsorption capacities of ZnO-rGO/CMF for soybean oil, petroleum, gasoline, DMF, acetone, and n-hexane were 120.2, 109.6, 91.7, 65.5, 50.0, and 42.2 g/g, respectively. Notably, the adsorption capacity for soybean oil surpasses that of most previously reported MF-derived materials listed in Table 1.

In addition to its high adsorption capacity, the reusability of ZnO-rGO/CMF is crucial for practical applications. The cyclic performance of ZnO-rGO/CMF was evaluated using a mechanical adsorption-squeezing-drying method, with soybean oil, n-hexane, gasoline, acetone, DMF, and petroleum as model adsorbates. The adsorption capacities for petroleum, gasoline, DMF, acetone, and n-hexane decreased from 109.6 to 90.2 g/g, 91.7 to 75.9 g/g, 65.5 to 53.4 g/g, 50.0 to 42.6 g/g, and 42.2 to 33.8 g/g, respectively, corresponding to retention rates of 82.2%, 82.7%, 81.5%, 85.2%, and 80.4% (Fig. 5g). After 20 adsorption-squeezing-drying cycles, the adsorption capacity for soybean oil decreased from 120.2 to 102 g/g, retaining 84.9% of its initial capacity (Fig. 5h). These results demonstrate that ZnO-rGO/CMF has high utility for the recovery of oils and organic solvents.

3.2.4 Flame retardant performance

MF, with its high nitrogen content, is considered a promising flame-retardant material, offering advantages for the remediation of oil spills and organic pollutants. The flame-retardancy test results are shown in Fig. 6a and 6b. Pristine MF burned rapidly upon exposure to a flame, and its structure collapsed after 50 s of combustion (Fig. 6a). In contrast, ZnO-rGO/CMF maintained its structural integrity even after 75 s of combustion, demonstrating excellent flame-retardant performance (Fig. 6b). As shown in Fig. 6c, ZnO-rGO/CMF retained more than 50% of its residual mass at 900 °C, indicating excellent thermal stability at high temperatures. After 5 combustion cycles, the adsorption capacity of ZnO-rGO/CMF for gasoline decreased from 89.2 g/g in the 1st cycle to 61.9 g/g in the 5th cycle, corresponding to a retention rate of over 67.5%. These results confirm the good reusability of ZnO-rGO/CMF under high-temperature conditions (Fig. 6d). After 5 consecutive 10 s combustion tests, no open flame or molten dripping was observed, and the sample was not burned through (Fig. S4). According to the UL-94 flammability standard, the sample achieved a 5VA rating, demonstrating outstanding flame retardancy.

The CMF framework derived from melamine foam carbonization provides a macroporous architecture that serves as a stable substrate for subsequent

Table 1 The performance of different absorbents

Absorbent	WCA/(°)	Adsorption capacity/(g/g)	Refs.
C_{16}TMS/PAL-VSiO_2/MS	154.1	70	[28]
SA@P25@SiO_2@MS	151.0	98	[29]
PU@PDA@SiO_2-Fe_3O_4-PDMS	151.3	28-29	[30]
PNiMFO10	164.0	132	[31]
PC/MF	159.3±1.9	80-84	[32]
MWCNT/MF	156.4±1.6	77-91	[32]
AGO-L-MF	132.2	69	[33]
Silane-MXene@MF	157.4	100	[34]
CAC-PDA@MF	159.5±2.0	72-79	[35]
BMCF	162.0	95	[36]
MTMS-C-PU	160.2±1.4	57-66	[37]
MS@PDA/LMs@TiO_2	160.3	49	[38]
ZnO-rGO/CMF	151.5	120	This work

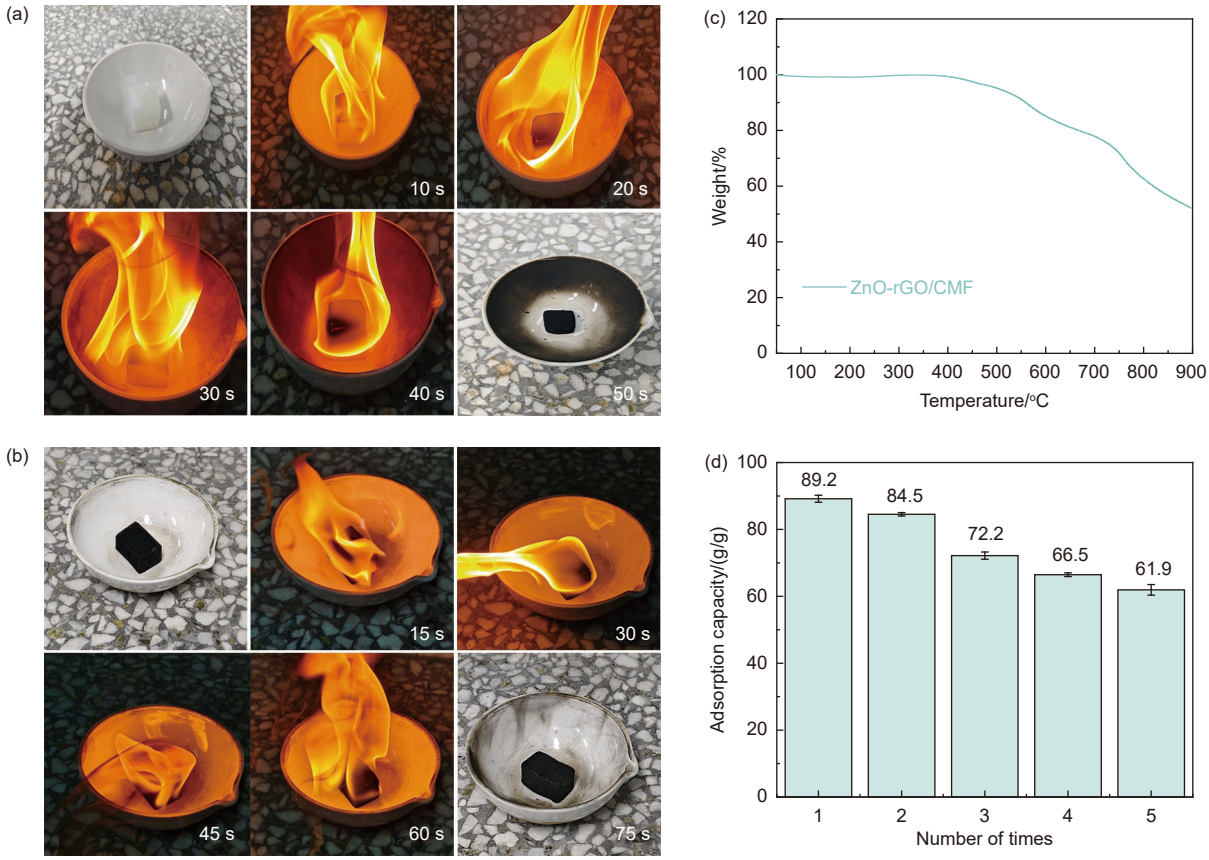

Fig. 6 (a, b) Flame retardancy test processes of pristine MF and ZnO-rGO/CMF. (c) Thermogravimetric analysis (TGA) curve of ZnO-rGO/CMF. (d) Changes in adsorption capacity of ZnO-rGO/CMF for target substances after 5 combustion cycles

modification. rGO nanosheets introduce a microscale rough layer on the CMF framework, while ZnO nanoparticles generate nanoscale protrusions on the rGO surface. Together, they form a micro/nano hierarchical rough structure that mimics a lotus-leaf-inspired surface. This biomimetic structure facilitates air trapping at the solid-liquid interface, forming a stable air barrier that prevents direct contact between water and the material surface, while simultaneously providing abundant adsorption sites for oil molecules. As a result, both the oil adsorption capacity and selective oil-water separation performance are significantly enhanced.

For large-scale oil pollution scenarios, such as marine oil spills, the high adsorption capacity, rapid separation capability, and flame retardancy of ZnO-rGO/CMF enable efficient removal of petroleum contaminants, followed by safe and efficient incineration treatment. The structural integrity of the material is largely preserved after combustion, enabling repeated use and reducing overall treatment costs. Furthermore, the material can be regenerated through mechanical squeezing, further improving its economic feasibility. The excellent hydrophobicity of ZnO-rGO/CMF allows it to maintain stable oil-water separation performance even in the presence of trace pollutants, enabling adaptability to complex wastewater conditions. These combined advantages endow ZnO-rGO/CMF with significant potential for applications in marine oil spill remediation, industrial wastewater treatment, and organic solvent recovery.

4 Conclusion

In this work, a ZnO-rGO/CMF composite sponge was successfully fabricated by a simple and environmentally friendly two-step synthesis combined with pyrolysis. ZnO-rGO/CMF exhibited a water contact angle (WCA) of 151.5°, indicating excellent superhydrophobicity. Its superior oil-water separation performance was demonstrated through both static and

continuous separation experiments, with no residual oil droplets detected in the aqueous phase. ZnO-rGO/CMF exhibited outstanding adsorption capacities for various oils and organic solvents, ranging from 42.2 to 120.2 g/g, and maintained stable performance after repeated use. Furthermore, ZnO-rGO/CMF demonstrated excellent mechanical stability, flame retardancy, and reusability. The preparation process avoids the use of toxic reagents, making it environmentally friendly and suitable for large-scale production. Benefiting from low-cost raw materials, a facile synthesis route, and scalability, this composite sponge represents a promising candidate for practical applications. It provides a viable material platform for environmental remediation, particularly in oil spill cleanup and industrial oily wastewater treatment.

Acknowledgements

This work was financially supported by the Graduate Innovation Research Project of Harbin Normal University (HSDSSCX2025-22), the Natural Science Foundation of Heilongjiang Province (PL2025B010) and the Basic Research of Outstanding Young Teachers in Heilongjiang Province (YQJH2025114).

References

[1] Meng Y, Zhou X, Huang Z, et al. Pumping with modified polyurethane sponges: A rapid oil spill treatment technology[J]. Korean Journal of Chemical Engineering, 2024, 41(7): 2133-2142.

[2] Wang F, Zhang H, Sun Y, et al. Superhydrophilic quaternized calcium alginate based aerogel membrane for oil-water separation and removal of bacteria and dyes[J]. International Journal of Biological Macromolecules, 2023, 227: 1141-1150.

[3] Li H, Zhu X, Zhao J, et al. Emerging adsorbents: Applications of sodium alginate/graphene oxide composite materials in wastewater treatment[J]. Journal of Water Process Engineering, 2024, 59: 105100.

[4] Irfan M, Lakshmi C N, Singh N, et al. Superhydrophobic polyurethane sponge modified with polydimethylsiloxane/zinc oxide-rGO for efficient oil or organic solvent/water separation[J]. Materials Letters, 2023, 348: 134668.

[5] Erfani H, Madhu N R, Khodayari S, et al. Separation and removal of oil from water/wastewater in the oil industry: A review[J]. Environmental Technology Reviews, 2024, 13(1): 325-343.

[6] Okoro O, Papineau I, Solliec M, et al. Performance of conventional drinking water treatment following dispersant remediation of an oil spill in surface water[J]. Science of the Total Environment, 2021, 801: 149583.

[7] Couto C R R de A, Assis D C de, Jurelevicius D L. Chemical and biological dispersants differently affect the bacterial communities of uncontaminated and oil-contaminated marine water[J]. Brazilian Journal of Microbiology, 2020, 51(2): 691-700.

[8] Duarte H, Aliaño-González M J, Romano A, et al. Advancements in detection and mitigation strategies for petroleum-derived contaminants in aquatic environments: A comprehensive review[J]. Sensors, 2024, 24(11): 3284.

[9] Muvel H, Jindal M K, Tewari P K, et al. Minimizing oil pollution: A review of current status and its treatment options[J]. RSC Sustainability, 2025, 3(9): 3681-3723.

[10] Rios-Miguel A B, van Bergen T J, Zillien C, et al. Predicting and improving the microbial removal of organic micropollutants during wastewater treatment: A review[J]. Chemosphere, 2023, 333: 138908.

[11] Heidari M K, Fouladi M, Sooreh H A, et al. Superhydrophobic and super-oleophilic natural sponge sorbent for crude oil/water separation[J]. Journal of Water Process Engineering, 2022, 48: 102783.

[12] Shen J, Yuan Y Z, Yu H M, et al. Smart wood membrane with reversible photo-responsive wettability for intelligent oil-water separation[J]. Chemical Engineering Journal, 2026, 531: 173904.

[13] Xu C, He H, Wang Y, et al. Superhydrophobic sponge-like chitosan/CNTs/silica composite for selective oil absorption and efficient separation of water-in-oil emulsion[J]. Carbohydrate Polymers, 2025, 353: 123256.

[14] Zhang B, Xue X, Zhao L, et al. Transparent superhydrophobic and self-cleaning coating[J]. Polymers, 2024, 16(13): 1876.

[15] Sha X, Chen L, Jia Y, et al. Preparation and properties of sustainable superhydrophobic cotton fabrics modified with lignin

nanoparticles, tannic acid and methyltrimethoxysilane[J]. Chemical Engineering Journal, 2024, 499: 1385-8947.

[16] Li Y, Li X, Xu L, et al. Facile construction of superhydrophobic/superoleophilic melamine sponges with durability and antifouling for selective oil absorption and effective oil/water separation[J]. Journal of Environmental Chemical Engineering, 2024, 12(2): 111919.

[17] Xiang W, Guo Z. Nonflammable, robust and recyclable hydrophobic zeolitic imidazolate frameworks/sponge with high oil absorption capacity for efficient oil/water separation[J]. Colloids and Surfaces A: Physicochemical and Engineering Aspects, 2022, 650: 129570.

[18] Zhang H, Li G, Huang B, et al. A new strategy for efficient adsorption-low fire risk for oil-water separation remediation without hydrophobic coatings: CoFeNi-PBA catalytic carbonization of melamine sponges[J]. Chemical Engineering Journal, 2025, 162730. https://doi.org/10.1016/j.cej.2025.162730.

[19] Niu H, Li J, Qiang Z, Ren J. Versatile and cost-efficient cleanup of viscous crude oil by an elastic carbon sorbent from direct pyrolysis of a melamine foam[J]. Journal of Materials Chemistry A, 2021, 9(18): 11268-11277.

[20] Zhang J Y, Wang P, Wen H, et al. Polymer brush-grafted cotton with petal-like microstructure as superhydrophobic and self-cleaning adsorbents for oil/water separation[J]. Colloids and Surfaces A Physicochemical and Engineering Aspects, 2021, 621: 126548.

[21] Feng Z, Xu Y, Yue W, et al. Recent progress in the use of graphene/polymer composites to remove oil contaminants from water[J]. New Carbon Materials, 2021, 36(2): 235-252.

[22] Duman O, Diker C Ö, Tunç S. Development of highly hydrophobic and superoleophilic fluoro organothiol-coated carbonized melamine sponge/rGO composite absorbent material for the efficient and selective absorption of oily substances from aqueous environments[J]. Journal of Environmental Chemical Engineering, 2021, 9(2): 105093.

[23] Guo L, Wen Y, Li F, et al. A novel approach for oil/water separation: Integrating nano-ZnO with graphene oxide membranes via dopamine and KH550[J]. Surfaces and Interfaces, 2024, 51: 104727.

[24] Li M, Li Q, Xu M, et al. Amphiphilic engineering of reduced graphene oxides using a carbon nitride coating for superior removal of organic pollutants from wastewater[J]. Carbon, 2021, 184: 479-491.

[25] Neto A J P, Fileti E E. Elucidating the amphiphilic character of graphene oxide[J]. Physical Chemistry Chemical Physics, 2018, 20(14): 9507-9515.

[26] Selim M S, El-Safty S A, Abbas M A, et al. Facile design of graphene oxide-ZnO nanorod-based ternary nanocomposite as a superhydrophobic and corrosion-barrier coating[J]. Colloids and Surfaces A: Physicochemical and Engineering Aspects, 2021, 611: 125793.

[27] Zhang X, Zhang J, Gong X, et al. Hybrid structured photothermal superhydrophobic copper foam for fast adsorption of highly viscous crude oil[J]. Langmuir, 2025, 41(28): 18674-18681.

[28] Zhang R, Zhou Z, Ge W, et al. Superhydrophobic sponge with the rod-spherical microstructure via palygorskite-catalyzed hydrolysis and condensation of vinyltriethoxysilane for oil-water separation[J]. Applied Clay Science, 2020, 199: 105872.

[29] Wang X, Quan Q, Piao H, et al. Green fabrication of superhydrophobic melamine hollow sponge tube for effective NAPL treatment[J]. Journal of Environmental Chemical Engineering, 2025: 117195. https://doi.org/10.1016/j.jece.2025.117195.

[30] Hu C, Xue T, Ma R, et al. Fabrication of biomimetic polyurethane sponges with superhydrophobic, magnetic response and flame retardant properties for efficient oil-water separation[J]. Journal of Environmental Chemical Engineering, 2025, 13(3): 116230.

[31] Okutan M. Ni induced superhydrophobic melamine foam sorbent for cleanup of oils/organic solvents[J]. Polymer Bulletin, 2023, 80(8): 9383-9407.

[32] Shayesteh H, Khosrowshahi M S, Mashhadimoslem H, et al. Durable superhydrophobic/superoleophilic melamine foam based on biomass-derived porous carbon and multi-walled carbon nanotube for oil/water separation[J]. Scientific Reports, 2023, 13(1): 4515.

[33] Yun H, Park S, Choi J, et al. Melamine and hydrophobic graphene composite foam with lignin as a green connector for oil-water separation applications[J]. Reactive and Functional Polymers, 2025, 209: 106173.

[34] Wang W, Song X, Xie Y, et al. A study on the preparation of superhydrophobic Silane-MXene modified melamine foam and its oil-water separation performance[J]. Frontiers in Materials, 2023, 10: 1277247.

[35] He L, Qi X, Wei W, et al. Biomass-activated carbon-based superhydrophobic sponge with photothermal properties for adsorptive separation of waste oil[J]. Journal of Hazardous Materials, 2024, 477: 135222.

[36] Zhao J, Li Q, Wang Q, et al. Facile construction of robust and powerful biochar-decorated porous foams with super-wettability for automatic and continuous oil spill remediation[J]. Industrial & Engineering Chemistry Research, 2023, 62(17): 6697-6706.

[37] Manoj T, Thomas S, Sobhan C B. Superhydrophobic/superoleophilic oil absorbing flame-retardant and photothermally active biochar-based polyurethane sponge[J]. Journal of Materials Engineering and Performance, 2025: 1-14. https://doi.org/10.1007/s11665-025-12774-2.

[38] Qiao L, Zhou Z, Wang M, et al. Lignin Microsphere/TiO_2 composite-based melamine sponge with superhydrophobic and photothermal properties for oil/water separation and anti-icing[J]. Langmuir, 2025, 41(21): 13233-13248.